
Projected Stein Variational Gradient Descent

Peng Chen **Omar Ghattas**
Oden Institute for Computational Engineering and Sciences
The University of Texas at Austin
Austin, TX 78712.
{peng, omar}@oden.utexas.edu

Abstract

The curse of dimensionality is a longstanding challenge in Bayesian inference in high dimensions. In this work, we propose a projected Stein variational gradient descent (pSVGD) method to overcome this challenge by exploiting the fundamental property of intrinsic low dimensionality of the data informed subspace stemming from ill-posedness of such problems. We adaptively construct the subspace using a gradient information matrix of the log-likelihood, and apply pSVGD to the much lower-dimensional coefficients of the parameter projection. The method is demonstrated to be more accurate and efficient than SVGD. It is also shown to be more scalable with respect to the number of parameters, samples, data points, and processor cores via experiments with parameters dimensions ranging from the hundreds to the tens of thousands.

1 Introduction

Given observation data for a system with unknown parameters, Bayesian inference provides an optimal probability framework for learning the parameters by updating their prior distribution to a posterior distribution. However, many conventional methods for solving high-dimensional Bayesian inference problems face the curse of dimensionality, i.e., the computational complexity grows rapidly, often exponentially, with respect to (w.r.t.) the number of parameters. To address the curse of dimensionality, the intrinsic properties of the posterior distribution, such as its smoothness, sparsity, and intrinsic low-dimensionality, have been exploited to reduce the parameter correlation and develop efficient methods whose complexity grows slowly or remains the same with increasing dimension. By exploiting the geometry of the log-likelihood function, accelerated Markov chain Monte Carlo (MCMC) methods have been developed to reduce the sample correlation or increase effective sample size independent of the dimension [18, 22, 24, 14, 15, 2]. Nevertheless, these random and essentially serial sampling methods remain prohibitive for large-scale inference problems with expensive likelihoods. Deterministic methods using sparse quadratures [29, 27, 8, 9] were shown to converge rapidly with dimension-independent rates for problems with smooth and sparse posteriors. However, for posteriors lacking smoothness or sparsity, the convergence deteriorates significantly, despite incorporation of Hessian-based transformations [28, 10].

Transport-based variational inference is another type of deterministic method that seeks a transport map in a function space (represented by, e.g., polynomials, kernels, or neural networks) that pushes the prior to the posterior by minimizing the difference between the transported prior and the posterior, measured in, e.g., Kullback–Leibler divergence [23, 21, 4, 3, 17]. In particular, kernel-based Stein variational methods, using gradient-based (SVGD) [21, 13, 20] and Hessian-based (SVN) [16, 32] optimization methods, are shown to achieve fast convergence in relatively low dimensions. Nonetheless, the convergence and accuracy of these methods deteriorates in high dimensions due to the curse of dimensionality in kernel representation. This can be partially addressed by a localized

SVGD on Markov blankets, which relies on conditional independence of the target distribution [34, 31], or by parameter projection for dimension reduction in pSVN [12] and lazy maps [3].

Contributions: Here, we propose, analyze, and apply a projected SVGD method to tackle the curse of dimensionality for high-dimensional nonlinear Bayesian inference problems, which relies on the fundamental property that the posterior effectively differs from the prior only in a low-dimensional subspace of high-dimensional parameters, see [6, 30, 19, 15, 10, 11, 7, 3, 12] and references therein. Specifically, our contributions are: (1) we propose dimension reduction by projecting the parameters to a low-dimensional subspace constructed using the gradient of the log-likelihood, and push the prior samples of the projection coefficients to their posterior by pSVGD; (2) we prove the equivalence of the projected transport in the coefficient space and the transport in the projected parameter space; (3) we propose adaptive and parallel algorithms to efficiently approximate the optimal profile function and the gradient information matrix for the construction of the subspace; and (4) we demonstrate the accuracy (compared to SVGD) and scalability of pSVGD w.r.t. the number of parameters, samples, data points, and processor cores by classical high-dimensional Bayesian inference problems.

The major differences of this work compared to pSVN [12] are: (1) pSVGD uses only gradient information of the log-likelihood, which is available for many models, while pSVN requires Hessian information, which is challenging for complex models and codes in practical applications; (2) the upper bound for the projection error w.r.t. the posterior is sharper than that for pSVN; (3) we prove the equivalence of the projected transport for the coefficient and the transport for the projected parameters; (4) we also test new benchmark examples and investigate the convergence of pSVGD w.r.t. the number of parameters and the scalability of pSVGD w.r.t. the number of data points.

2 Preliminaries

Let $x \in \mathbb{R}^d$ denote a random parameter of dimension $d \in \mathbb{N}$, which has a continuous prior density $p_0 : \mathbb{R}^d \rightarrow \mathbb{R}$. Let $y = \{y_i\}_{i=1}^s$ denote a set of i.i.d. observation data. Let $f(x) := \prod_{i=1}^s p(y_i|x)$ denote, up to a multiplicative constant, a continuous likelihood of y at given x . Then the posterior density of parameter x conditioned on data y , denoted as $p(\cdot) : \mathbb{R}^d \rightarrow \mathbb{R}$, is given by Bayes' rule as

$$p(x) = \frac{1}{Z} f(x) p_0(x), \quad (1)$$

where Z is the normalization constant defined as

$$Z = \int_{\mathbb{R}^d} f(x) p_0(x) dx, \quad (2)$$

whose computation is typically intractable, especially for a large d . The central task of Bayesian inference is to draw samples of parameter x from its posterior with density p , and compute some statistical quantity of interest, e.g., the mean and variance of the parameter x or some function of x .

SVGD is one type of variational inference method that seeks an approximation of the posterior density p by a function q^* in a predefined function set \mathcal{Q} , which is realized by minimizing the Kullback–Leibler (KL) divergence that measures the difference between two densities, i.e.,

$$q^* = \arg \min_{q \in \mathcal{Q}} D_{\text{KL}}(q|p), \quad (3)$$

where $D_{\text{KL}}(q|p) = \mathbb{E}_{x \sim q}[\log(q/p)]$, i.e., the average of $\log(q/p)$ with respect to the density q , which vanishes when $q = p$. In particular, a transport based function set is considered as $\mathcal{Q} = \{T_{\#} p_0 : T \in \mathcal{T}\}$, where $T_{\#}$ is a pushforward map that pushes the prior density to a new density $q := T_{\#} p_0$ through an invertible transport map $T(\cdot) : \mathbb{R}^d \rightarrow \mathbb{R}^d$ in a space \mathcal{T} . Let T be given by

$$T(x) = x + \epsilon \phi(x), \quad (4)$$

where $\phi : \mathbb{R}^d \rightarrow \mathbb{R}^d$ is a differentiable perturbation map w.r.t. x , and $\epsilon > 0$ is small enough so that T is invertible. It is shown in [21] that

$$\nabla_{\epsilon} D_{\text{KL}}(T_{\#} p_0|p) \Big|_{\epsilon=0} = -\mathbb{E}_{x \sim p_0}[\text{trace}(\mathcal{A}_p \phi(x))], \quad (5)$$

where \mathcal{A}_p is the Stein operator given by

$$\mathcal{A}_p \phi(x) = \nabla_x \log p(x) \phi(x)^T + \nabla_x \phi(x). \quad (6)$$

Based on this result, a practical SVGD algorithm was developed in [21] by choosing the space $\mathcal{T} = (\mathcal{H}_d)^d = \mathcal{H}_d \times \dots \times \mathcal{H}_d$, a tensor product of a reproducing kernel Hilbert space (RKHS) \mathcal{H}_d with kernel $k(\cdot, \cdot) : \mathbb{R}^d \times \mathbb{R}^d \rightarrow \mathbb{R}$. SVGD updates samples x_1^0, \dots, x_N^0 drawn from the prior p_0 as

$$x_m^{\ell+1} = x_m^\ell + \epsilon_\ell \hat{\phi}_\ell^*(x_m^\ell), \quad m = 1, \dots, N, \ell = 0, 1, \dots \quad (7)$$

where ϵ_ℓ is a step size or learning rate, and $\hat{\phi}_\ell^*(x_m^\ell)$ is an approximate steepest direction given by

$$\hat{\phi}_\ell^*(x_m^\ell) = \frac{1}{N} \sum_{n=1}^N \nabla_{x_n^\ell} \log p(x_n^\ell) k(x_n^\ell, x_m^\ell) + \nabla_{x_n^\ell} k(x_n^\ell, x_m^\ell). \quad (8)$$

The kernel k plays a critical role in pushing the samples to the posterior. One choice is Gaussian

$$k(x, x') = \exp\left(-\frac{\|x - x'\|_2^2}{h}\right), \quad (9)$$

where h is the bandwidth, e.g., $h = \text{med}^2 / \log(N)$ with med representing the median of sample distances [21]. However, it is known that the kernel suffers from the *curse of dimensionality* for large d [25, 34, 31], which leads to samples not representative of the posterior, as observed in [34, 31].

3 Projected Stein Variational Gradient Descent

To tackle the curse of dimensionality of SVGD, we exploit one fundamental property of many high-dimensional Bayesian inference problems — the posterior only effectively differs from the prior in a relatively low-dimensional subspace due to the ill-posedness or over-parametrization of the inference problems, see many examples and some proofs in, e.g., [1, 5, 6, 30, 19, 15, 10, 11, 7, 3, 12].

3.1 Dimension reduction by projection

By $H \in \mathbb{R}^{d \times d}$ we denote a gradient information matrix, which is defined as the average of the outer product of the gradient of the log-likelihood w.r.t. the posterior, i.e.,

$$H = \int_{\mathbb{R}^d} (\nabla_x \log f(x)) (\nabla_x \log f(x))^T p(x) dx. \quad (10)$$

By $(\lambda_i, \psi_i)_{i=1}^r$ we denote the dominant eigenpairs of (H, Γ) , with Γ representing the covariance of the parameter x w.r.t. its prior, i.e., $(\lambda_i, \psi_i)_{i=1}^r$ correspond to the r largest eigenvalues $\lambda_1 \geq \dots \geq \lambda_r$,

$$H\psi_i = \lambda_i \Gamma \psi_i. \quad (11)$$

Given H , which is practically computed in Section 3.3, the generalized eigenvalue problem (11) can be efficiently solved by a randomized algorithm [26] that only requires $O(r)$ matrix vector product. We make the following key observation: *The eigenvalue λ_i measures the sensitivity of the data w.r.t. the parameters along direction ψ_i , i.e., the data mostly inform parameters in directions ψ_i corresponding to large eigenvalues λ_i . For i with small λ_i , close to zero, the variation of the likelihood f in direction ψ_i is negligible, so the posterior is close to the prior in direction ψ_i .*

We define a linear projector of rank r , $P_r : \mathbb{R}^d \rightarrow \mathbb{R}^d$, as

$$P_r x := \sum_{i=1}^r \psi_i \psi_i^T x = \Psi_r w, \quad \forall x \in \mathbb{R}^d, \quad (12)$$

where $\Psi_r := (\psi_1, \dots, \psi_r) \in \mathbb{R}^{d \times r}$ represents the projection matrix and $w := (w_1, \dots, w_r)^T \in \mathbb{R}^r$ is the coefficient vector with element $w_i := \psi_i^T x$ for $i = 1, \dots, r$. For this projection, we seek a *profile function* $g : \mathbb{R}^d \rightarrow \mathbb{R}$ such that $g(P_r x)$ is a good approximation of the likelihood function $f(x)$. For a given profile function, we define a projected density $p_r : \mathbb{R}^d \rightarrow \mathbb{R}$ as

$$p_r(x) := \frac{1}{Z_r} g(P_r x) p_0(x), \quad (13)$$

where $Z_r := \mathbb{E}_{x \sim p_0}[g(P_r x)]$. It is shown in [33] that an optimal profile function g^* exists such that

$$D_{\text{KL}}(p|p_r^*) \leq D_{\text{KL}}(p|p_r), \quad (14)$$

where p_r^* is defined as in (13) with an optimal profile function g^* . Moreover, under certain mild assumptions for the prior (sub-Gaussian) and the likelihood function (whose gradient has the second moment w.r.t. the prior), the upper bound is shown (sharper than that for pSVN in [12]) as

$$D_{\text{KL}}(p|p_r^*) \leq \frac{\gamma}{2} \sum_{i=r+1}^d \lambda_i, \quad (15)$$

for a constant $\gamma > 0$ independent of r , which implies small projection error for the posterior when λ_i decay fast. The optimal profile function g^* is nothing but the marginal likelihood given by

$$g^*(P_r x) = \int_{X_\perp} f(P_r x + \xi) p_0^\perp(\xi | P_r x) d\xi, \quad (16)$$

where X_\perp is the complement of the subspace X_r spanned by ψ_1, \dots, ψ_r , and

$$p_0^\perp(\xi | P_r x) = p_0(P_r x + \xi) / p_0^r(P_r x) \text{ with } p_0^r(P_r x) = \int_{X_\perp} p_0(P_r x + \xi) d\xi. \quad (17)$$

We defer a practical computation of the optimal profile function to Section 3.3.

3.2 Projected Stein Variational Gradient Descent

By the projection (12), we consider a decomposition of the prior for the parameter $x = x^r + x^\perp$ as

$$p_0(x) = p_0^r(x^r) p_0^\perp(x^\perp | x^r), \quad (18)$$

where the marginals p_0^r and p_0^\perp are defined in (17). Moreover, since p_0^r only depends on $x^r = P_r x = \Psi_r w$, we define a prior density for w as

$$\pi_0(w) = p_0^r(\Psi_r w). \quad (19)$$

Then we define a joint (posterior) density for w at the optimal profile function $g = g^*$ in (13) as

$$\pi(w) = \frac{1}{Z_w} g(\Psi_r w) \pi_0(w), \quad (20)$$

where the normalization constant $Z_w = E_{w \sim \pi_0} [g(\Psi_r w)]$. It is easy to see that $Z_w = Z_r$, where Z_r is in (13), and the projected density in (13) can be written as

$$p_r(x) = \pi(w) p_0^\perp(x^\perp | \Psi_r w). \quad (21)$$

Therefore, to sample x from p_r , we only need to sample w from π and x^\perp from $p_0^\perp(x^\perp | \Psi_r w)$.

To sample from the posterior π in (20), we employ the SVGD method presented in Section 2 in the coefficient space \mathbb{R}^r , with $r < d$. Specifically, we define a projected transport map $T^r : \mathbb{R}^r \rightarrow \mathbb{R}^r$ as

$$T^r(w) = w + \epsilon \phi^r(w), \quad (22)$$

with a differentiable perturbation map $\phi^r : \mathbb{R}^r \rightarrow \mathbb{R}^r$, and a small enough $\epsilon > 0$ such that T^r is invertible. Following the argument in [21] on the result (5) for SVGD, we obtain

$$\nabla_\epsilon D_{\text{KL}}(T_\#^r \pi_0 | \pi) \Big|_{\epsilon=0} = -\mathbb{E}_{w \sim \pi_0} [\text{trace}(\mathcal{A}_\pi \phi^r(w))], \quad (23)$$

where \mathcal{A}_π is the Stein operator for π given by

$$\mathcal{A}_\pi \phi^r(w) = \nabla_w \log \pi(w) \phi^r(w)^T + \nabla_w \phi^r(w). \quad (24)$$

Using a tensor product of RKHS \mathcal{H}_r with kernel $k^r(\cdot, \cdot) : \mathbb{R}^r \times \mathbb{R}^r \rightarrow \mathbb{R}$ for the approximation of $\phi^r \in (\mathcal{H}_r)^r = \mathcal{H}_r \times \dots \times \mathcal{H}_r$, a SVGD update of the samples w_1^0, \dots, w_N^0 from $\pi_0(w)$ leads to

$$w_m^{\ell+1} = w_m^\ell + \epsilon_\ell \hat{\phi}_\ell^{r,*}(w_m^\ell), \quad m = 1, \dots, N, \ell = 0, 1, \dots, \quad (25)$$

with a step size ϵ_ℓ and an approximate steepest direction

$$\hat{\phi}_\ell^{r,*}(w_m^\ell) = \frac{1}{N} \sum_{n=1}^N \nabla_{w_n^\ell} \log \pi(w_n^\ell) k^r(w_n^\ell, w_m^\ell) + \nabla_{w_n^\ell} k^r(w_n^\ell, w_m^\ell). \quad (26)$$

The kernel k^r can be specified as in (9), i.e.,

$$k^r(w, w') = \exp\left(-\frac{\|w - w'\|_2^2}{h}\right). \quad (27)$$

To account for data impact in different directions ψ_1, \dots, ψ_r informed by the eigenvalues of (11), we propose to replace $\|w - w'\|_2^2$ in (27) by $(w - w')^T(\Lambda + I)(w - w')$ with $\Lambda = \text{diag}(\lambda_1, \dots, \lambda_r)$ for the likelihood and I for the prior.

The following theorem, proved in Appendix A, gives $\nabla_w \log \pi(w)$ and the connection between pSVGd for the coefficient w and SVGd for the projected parameter $P_r x$ under certain conditions.

Theorem 1. *The gradient of the posterior π in (20) is given by*

$$\nabla_w \log \pi(w) = \Psi_r^T \left(\frac{\nabla_x g(P_r x)}{g(P_r x)} + \frac{\nabla_x p_0^r(P_r x)}{p_0^r(P_r x)} \right). \quad (28)$$

Moreover, with the kernel $k^r(\cdot, \cdot) : \mathbb{R}^r \times \mathbb{R}^r \rightarrow \mathbb{R}$ defined in (27) and $k(\cdot, \cdot) : \mathbb{R}^d \times \mathbb{R}^d \rightarrow \mathbb{R}$ defined in (9), if $p_0^r(P_r x) = p_0(P_r x)$, for example p_0 is Gaussian, we have the equivalence of the projected transport map T^r for the coefficient w and the transport map T for the projected parameter $P_r x$, as

$$T^r(w) = \Psi_r^T T(P_r x). \quad (29)$$

In particular, we have

$$\nabla_w \log \pi(w) = \Psi_r^T \nabla_x \log p_r(P_r x). \quad (30)$$

3.3 Practical algorithms

Sampling from the projected density $p_r^*(x)$ defined in (13) for the optimal profile function g^* in (16) involves, by the decomposition (21), sampling w from the posterior π by pSVGd and sampling x^\perp from the conditional distribution with density $p_0^\perp(x^\perp | \Psi_r w)$. The sampling is impractical because of two challenges: (1) Both $p_0^\perp(x^\perp | \Psi_r w)$ and g^* in (16) involve high-dimensional integrals. (2) The matrix H defined in (10) for the construction of the basis ψ_1, \dots, ψ_r involves integration w.r.t. the posterior distribution of the parameter x . However, drawing samples from the posterior to evaluate the integral turns out to be the central task of the Bayesian inference.

The first challenge can be practically addressed by using the property — the posterior distribution only effectively differs from the prior in the dominant subspace X_r , or the variation of likelihood f in the complement subspace X_\perp is negligible. Therefore, for any sample x_n^0 drawn from the prior p_0 , $n = 1, \dots, N$, we compute $x_n^\perp = x_n^0 - P_r x_n^0$ and freeze it for given P_r as a sample from $p_0^\perp(x^\perp | P_r x)$. Moreover, at sample x_n^ℓ we approximate the optimal profile function g^* in (16) as

$$g^*(P_r x_n^\ell) \approx f(P_r x_n^\ell + x_n^\perp), \quad (31)$$

which is equivalent to using one sample x_n^\perp to approximate the integral (16) because the variation of f in the complement subspace X_\perp is small. This is used in computing $\nabla_w \log \pi(w)$ in (28).

Given the projector P_r with basis Ψ_r , we summarize the pSVGd transport of samples in Algorithm 1. In particular, by leveraging the property that the samples can be updated in parallel, we implement a parallel version of pSVGd using MPI for information communication in K processor cores, each with N different samples, thus producing $M = NK$ different samples in total.

To construct the projector P_r with basis Ψ_r , we approximate H in (10) by

$$\hat{H} := \frac{1}{M} \sum_{m=1}^M \nabla_x \log f(x_m) (\nabla_x \log f(x_m))^T. \quad (32)$$

where x_1, \dots, x_M are supposed to be samples from the posterior, which are however not available at the beginning. We propose to adaptively construct the basis Ψ_r^ℓ with samples $x_1^\ell, \dots, x_M^\ell$ transported from the prior samples x_1^0, \dots, x_M^0 by pSVGd. This procedure is summarized in Algorithm 2. We remark that by the adaptive construction, we push the samples to their posterior in each subspace $X_r^{\ell_x}$ spanned by (possibly) different basis $\Psi_r^{\ell_x}$ with different r for different ℓ_x , during which the frozen samples x_n^\perp in Algorithm 1 are also updated at each step ℓ_x of Algorithm 2.

Algorithm 1 pSVGD in parallel

- 1: **Input:** samples $\{x_n^0\}_{n=1}^N$ in each of K cores, basis Ψ_r , maximum iteration L_{\max} , tolerance w_{tol} .
 - 2: **Output:** posterior samples $\{x_n^*\}_{n=1}^N$ in each core.
 - 3: Set $\ell = 0$, project $w_n^0 = \Psi_r^T x_n^0$, $x_n^\perp = x_n^0 - \Psi_r w_n^0$, and perform MPI_Allgather for $\{w_n^0\}_{n=1}^N$.
 - 4: **repeat**
 - 5: Compute gradients $\nabla_{w_n^\ell} \log \pi(w_n^\ell)$ by (28) for $n = 1, \dots, N$, and perform MPI_Allgather.
 - 6: Compute the kernel values $k^r(w_n^\ell, w_m^\ell)$ and their gradients $\nabla_{w_n^\ell} k^r(w_n^\ell, w_m^\ell)$ for $n = 1, \dots, NK$, $m = 1, \dots, N$, and perform MPI_Allgather for them.
 - 7: Update samples $w_m^{\ell+1}$ from w_m^ℓ by (25) and (26) for $m = 1, \dots, N$, with NK samples used for SAA in (26), and perform MPI_Allgather for $\{w_m^0\}_{m=1}^N$.
 - 8: Set $\ell \leftarrow \ell + 1$.
 - 9: **until** $\ell \geq L_{\max}$ or $\text{mean}(\|w_m^\ell - w_m^{\ell-1}\|_2) \leq w_{\text{tol}}$.
 - 10: Reconstruct samples $x_n^* = \Psi_r w_n^\ell + x_n^\perp$.
-

Algorithm 2 Adaptive pSVGD in parallel

- 1: **Input:** samples $\{x_n^0\}_{n=1}^N$ in each of K cores, $L_{\max}^x, L_{\max}^w, x_{\text{tol}}, w_{\text{tol}}$.
- 2: **Output:** posterior samples $\{x_n^*\}_{n=1}^N$ in each core.
- 3: Set $\ell_x = 0$.
- 4: **repeat**
- 5: Compute $\nabla_x \log f(x_n^{\ell_x})$ in (32) for $n = 1, \dots, N$ in each core, and perform MPI_Allgather.
- 6: Solve (11) with H approximated as in (32), with all $M = NK$ samples, to get bases $\Psi_r^{\ell_x}$.
- 7: Apply the pSVGD Algorithm 1, i.e.,

$$\{x_n^*\}_{n=1}^N = \text{pSVGD}(\{x_n^{\ell_x}\}_{n=1}^N, \Psi_r^{\ell_x}, L_{\max}^w, w_{\text{tol}}).$$

- 8: Set $\ell_x \leftarrow \ell_x + 1$ and $x_n^{\ell_x} = x_n^*$, $n = 1, \dots, N$.
 - 9: **until** $\ell_x \geq L_{\max}^x$ or $\text{mean}(\|x_m^{\ell_x} - x_m^{\ell_x-1}\|_X) \leq x_{\text{tol}}$.
-

4 Numerical Experiments

We present three Bayesian inference problems with high-dimensional parameters to demonstrate the accuracy of pSVGD compared to SVGD, and the convergence and scalability of pSVGD w.r.t. the number of parameters, samples, data points, and processor cores. A linear inference example, whose posterior is analytically given, is presented in Appendix B to demonstrate the accuracy of pSVGD. An application in COVID-19 to infer the social distancing effect given hospitalized data is presented in Appendix C. The code is available at <https://github.com/cpempire/pSVGD>.

4.1 Conditional diffusion process

We consider a high-dimensional model that is often used to test inference algorithms in high dimensions, e.g., Stein variational Newton in [16], which is discretized from a conditional diffusion process

$$du_t = \frac{10u(1-u^2)}{1+u^2} dt + dx_t, \quad t \in (0, 1], \quad (33)$$

with zero initial condition $u_0 = 0$. The forcing term $(x_t)_{t \geq 0}$ is a Brownian motion, whose prior is Gaussian with zero mean and covariance $C(t, t') = \min(t, t')$. We use Euler-Maruyama scheme with step size $\Delta t = 0.01$ for the discretization, which leads to dimension $d = 100$ for the discrete Brownian path x . We generate the data by first solving (33) at a true Brownian path x_{true} , and taking $y = (y_1, \dots, y_{20})$ with $y_i = u_{t_i} + \xi_i$ for equispaced t_1, \dots, t_{20} in $(0, 1]$ and additive noise $\xi_i \in N(0, \sigma^2)$ with $\sigma = 0.1$. We run SVGD and the adaptive pSVGD with line search for the learning rate, using $N = 128$ samples to infer x_{true} , where the subspace for pSVGD is updated every 10 iterations. The results are displayed in Figure 1. From the left we can see a fast decay of eigenvalues of (11), especially when the iteration number ℓ becomes big with the samples converging to the posterior, which indicates the existence of an intrinsic low-dimensional subspace. From the right we can observe that pSVGD leads to samples at which the solutions are much closer to the noisy data as

well as the true solution than that of SVGD. Moreover, the posterior mean of pSVGD is much closer to the true parameter with much tighter 90% confidence interval covering x_{true} than that of SVGD.

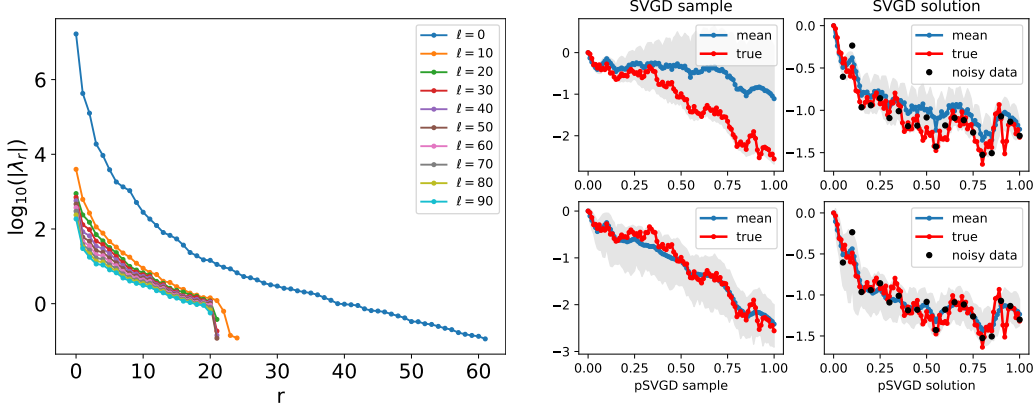


Figure 1: Left: Decay of the eigenvalues of (11) at different iteration numbers ℓ . Right: SVGD (top) and pSVGD (bottom) samples and solutions at iteration $\ell = 100$, including the synthetic true, posterior mean, 90% confidence interval in shadow, and noisy data points.

4.2 Bayesian logistic regression

We consider Bayesian logistic regression for binary classification of cancer and normal patterns for mass-spectrometric data with 10,000 attributes from <https://archive.ics.uci.edu/ml/datasets/Arcene>, which leads to $d = 10,000$ parameters (with i.i.d. uniform distribution as prior for Figure 2; Gaussian is also tested with similar results). We use 100 data for training and 100 for testing. We run pSVGD and SVGD with line search and 32 samples, with projection basis updated every 100 iterations. The results are shown in Figure 2. We can see a dramatic decay of the eigenvalues, which indicates an intrinsic dominant low dimensional subspace in which pSVGD effectively drives the samples to the posterior, and leads to more accurate prediction than that of SVGD. We remark that 32 samples in the estimate for the gradient information matrix in (32) are sufficient to capture the subspace since more samples lead to similar decay of eigenvalues as in Figure 2.

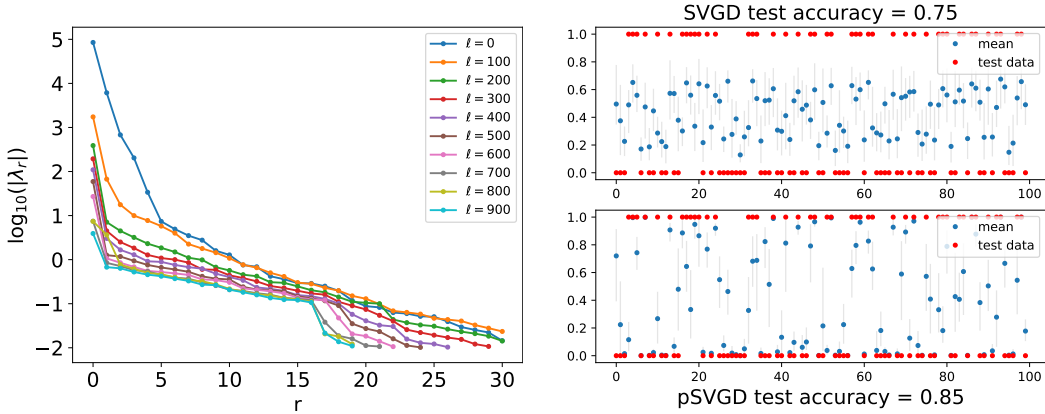


Figure 2: Left: Decay of the eigenvalues of (11) at different iteration numbers ℓ . Right: SVGD (top) and pSVGD (bottom) test data and prediction at iteration $\ell = 1000$, including posterior mean, 90% confidence interval in shadow. The 85% test accuracy for pSVGD is the same as for SVM from the data source file. The training time for pSVGD is 201 seconds compared to 477 seconds for SVGD.

4.3 Partial differential equation

In this example we consider an elliptic partial differential equation model (widely used in various fields, e.g., inference for permeability in groundwater flow, thermal conductivity in material science, electrical impedance in medical imaging, etc.), with a simplified form as

$$-\nabla \cdot (e^x \nabla u) = 0, \quad \text{in } (0, 1)^2, \quad (34)$$

which is imposed with Dirichlet boundary conditions $u = 1$ on the top boundary and $u = 0$ on bottom boundary, and homogeneous Neumann boundary conditions on the left and right boundaries. $\nabla \cdot$ is a divergence operator, and ∇ is a gradient operator. x and u are discretized by finite elements with piecewise linear elements in a uniform mesh of triangles of size d . $x \in \mathbb{R}^d$ and $u \in \mathbb{R}^d$ are the nodal values of x and u . We consider a Gaussian distribution for $x \in \mathcal{N}(0, \mathcal{C})$ with covariance $\mathcal{C} = (-0.1\Delta + I)^{-2}$, which leads to a Gaussian distribution for $x \sim \mathcal{N}(0, \Sigma_x)$, where $\Sigma_x \in \mathbb{R}^{d \times d}$ is discretized from \mathcal{C} . We consider a parameter-to-observable map $h(x) = O \circ S(x)$, where $S : x \rightarrow u$ is a nonlinear discrete solution map of the equation (34), $O : \mathbb{R}^d \rightarrow \mathbb{R}^s$ is a pointwise observation map at $s = 7 \times 7$ points equally distributed in $(0, 1)^2$. We consider an additive 5% noise $\xi \sim \mathcal{N}(0, \Sigma_\xi)$ with $\Sigma_\xi = \sigma^2 I$ and $\sigma = \max(|Ou|)/20$ for data $y = h(x) + \xi$.

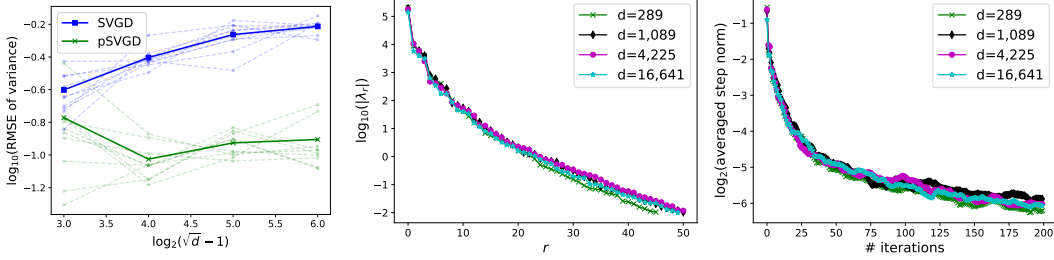


Figure 3: Left: RMSE of pointwise sample variance in L_2 -norm, with dimension $d = (2^n + 1)^2$, $n = 3, 4, 5, 6$. Middle: Scalability w.r.t. d by decay of eigenvalues λ_r w.r.t. r . Right: decay of the averaged step norm $\text{mean}_m \|w_m^{\ell+1} - w_m^\ell\|_2$ w.r.t. the number of iterations for different dimension d . We use a DILI-MCMC algorithm [15] to generate 10, 000 effective posterior samples and use them to compute a reference sample variance. We run SVGD and the adaptive pSVGd (with $\lambda_{r+1} < 10^{-2}$) using 256 samples and 200 iterations for different dimensions, both using line search to seek the step size ϵ_ℓ . The comparison of accuracy can be observed in the left of Figure 3. We can see that SVGD samples fail to capture the posterior distribution in high dimensions and become worse with increasing dimension, while pSVGd samples represent the posterior distribution well, measured by sample variance, and the approximation remains accurate with increasing dimension. The accuracy

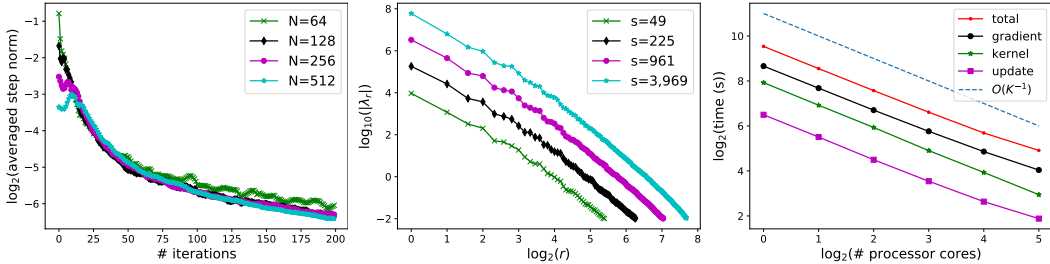


Figure 4: Scalability w.r.t. the number of (1) samples N by decay of the averaged step norm (left), (2) data points s by decay of eigenvalues (middle), and (3) processor cores K by decay of CPU time (for gradient including eigendecomposition (11), kernel, sample update, total) of pSVGd (right).

of pSVGd can be further demonstrated by the significant decay (about 7 orders of magnitude) of the eigenvalues for different dimensions in the middle of Figure 3. Only about 50 dimensions (with small relative projection error, about $\mathcal{E}_r < 10^{-6}$, committed in the posterior by (15)) are preserved out of from 289 to 16,641 dimensions, representing over $300\times$ dimension reduction for the last case. The similar decays of the eigenvalues λ_r in the projection rank r and the averaged step norm $\text{mean}_m \|w_m^{\ell+1} - w_m^\ell\|_2$ in the number of iterations shown in the right of Figure 3 imply that pSVGd is scalable w.r.t. the parameter dimension. Moreover, the similar decays for different sample size $N = 64, 128, 256, 512$ in the left of Figure 4 demonstrate that pSVGd is scalable w.r.t. the number of samples N . Furthermore, as displayed in the middle of Figure 4, with increasing number of i.i.d. observation data points $s = 7^2, 15^2, 31^2, 63^2$ in a refined mesh of size $d = 17^2, 33^2, 65^2, 129^2$, the eigenvalues decay at almost the same rate with similar relative projection error \mathcal{E}_r , and lead to similar reduction d/r for r such that $\lambda_{r+1} < 10^{-2}$, which implies weak scalability of pSVGd w.r.t. the number of data points. Lastly, from the right of Figure 4 by the nearly $O(K^{-1})$ decay of CPU time we can see that pSVGd achieves strong parallel scalability (in computing gradient, kernel, and sample update) w.r.t. the number of processor cores K for the same work with $KN = 1024$ samples.

5 Conclusions

We proposed a new algorithm — pSVGD for Bayesian inference in high dimensions to tackle the critical challenge of the curse of dimensionality. The projection error committed in the posterior can be bounded by the truncated (fast decaying) eigenvalues. We proved that pSVGD for the coefficient is equivalent to SVGD for the projected parameter under suitable assumptions. We demonstrated that pSVGD overcomes the curse of dimensionality for several high-dimensional Bayesian inference problems. In particular, we showed that pSVGD is scalable w.r.t. the number of parameters, samples, data points, and processor cores for a widely used benchmark problem in various scientific and engineering fields, which is crucial for solving high-dimensional and large-scale inference problems.

References

- [1] O. Bashir, K. Willcox, O. Ghattas, B. van Bloemen Waanders, and J. Hill. Hessian-based model reduction for large-scale systems with initial condition inputs. *International Journal for Numerical Methods in Engineering*, 73:844–868, 2008.
- [2] Alexandros Beskos, Mark Girolami, Shiwei Lan, Patrick E. Farrell, and Andrew M. Stuart. Geometric MCMC for infinite-dimensional inverse problems. *Journal of Computational Physics*, 335:327 – 351, 2017.
- [3] Daniele Bigoni, Olivier Zahm, Alessio Spantini, and Youssef Marzouk. Greedy inference with layers of lazy maps. *arXiv preprint arXiv:1906.00031*, 2019.
- [4] David M Blei, Alp Kucukelbir, and Jon D McAuliffe. Variational inference: A review for statisticians. *Journal of the American Statistical Association*, 112(518):859–877, 2017.
- [5] T. Bui-Thanh and O. Ghattas. Analysis of the Hessian for inverse scattering problems: I. Inverse shape scattering of acoustic waves. *Inverse Problems*, 28(5):055001, 2012.
- [6] T. Bui-Thanh, O. Ghattas, J. Martin, and G. Stadler. A computational framework for infinite-dimensional bayesian inverse problems part I: The linearized case, with application to global seismic inversion. *SIAM Journal on Scientific Computing*, 35(6):A2494–A2523, 2013.
- [7] Peng Chen and Omar Ghattas. Hessian-based sampling for high-dimensional model reduction. *International Journal for Uncertainty Quantification*, 9(2), 2019.
- [8] Peng Chen and Christoph Schwab. Sparse-grid, reduced-basis Bayesian inversion. *Computer Methods in Applied Mechanics and Engineering*, 297:84 – 115, 2015.
- [9] Peng Chen and Christoph Schwab. Sparse-grid, reduced-basis Bayesian inversion: Nonaffine-parametric nonlinear equations. *Journal of Computational Physics*, 316:470 – 503, 2016.
- [10] Peng Chen, Umberto Villa, and Omar Ghattas. Hessian-based adaptive sparse quadrature for infinite-dimensional Bayesian inverse problems. *Computer Methods in Applied Mechanics and Engineering*, 327:147–172, 2017.
- [11] Peng Chen, Umberto Villa, and Omar Ghattas. Taylor approximation and variance reduction for PDE-constrained optimal control problems under uncertainty. *Journal of Computational Physics*, 2019. To appear.
- [12] Peng Chen, Keyi Wu, Joshua Chen, Tom O’Leary-Roseberry, and Omar Ghattas. Projected Stein variational Newton: A fast and scalable Bayesian inference method in high dimensions. In *Advances in Neural Information Processing Systems*, pages 15104–15113, 2019.
- [13] Wilson Ye Chen, Lester Mackey, Jackson Gorham, François-Xavier Briol, and Chris J Oates. Stein points. *arXiv preprint arXiv:1803.10161*, 2018.
- [14] Paul G Constantine, Carson Kent, and Tan Bui-Thanh. Accelerating Markov chain Monte Carlo with active subspaces. *SIAM Journal on Scientific Computing*, 38(5):A2779–A2805, 2016.
- [15] Tiangang Cui, Kody JH Law, and Youssef M Marzouk. Dimension-independent likelihood-informed MCMC. *Journal of Computational Physics*, 304:109–137, 2016.
- [16] Gianluca Detommaso, Tiangang Cui, Youssef Marzouk, Alessio Spantini, and Robert Scheichl. A stein variational Newton method. In *Advances in Neural Information Processing Systems*, pages 9187–9197, 2018.

- [17] Gianluca Detommaso, Jakob Kruse, Lynton Ardizzone, Carsten Rother, Ullrich Köthe, and Robert Scheichl. HINT: Hierarchical invertible neural transport for general and sequential Bayesian inference. *arXiv preprint arXiv:1905.10687*, 2019.
- [18] Mark Girolami and Ben Calderhead. Riemann manifold Langevin and Hamiltonian Monte Carlo methods. *Journal of the Royal Statistical Society: Series B (Statistical Methodology)*, 73(2):123–214, 2011.
- [19] Tobin Isaac, Noemi Petra, Georg Stadler, and Omar Ghattas. Scalable and efficient algorithms for the propagation of uncertainty from data through inference to prediction for large-scale problems, with application to flow of the Antarctic ice sheet. *Journal of Computational Physics*, 296:348–368, September 2015.
- [20] Chang Liu and Jun Zhu. Riemannian Stein variational gradient descent for Bayesian inference. In *Thirty-Second AAAI Conference on Artificial Intelligence*, 2018.
- [21] Qiang Liu and Dilin Wang. Stein variational gradient descent: A general purpose Bayesian inference algorithm. In *Advances In Neural Information Processing Systems*, pages 2378–2386, 2016.
- [22] J. Martin, L.C. Wilcox, C. Burstedde, and O. Ghattas. A stochastic Newton MCMC method for large-scale statistical inverse problems with application to seismic inversion. *SIAM Journal on Scientific Computing*, 34(3):A1460–A1487, 2012.
- [23] Youssef Marzouk, Tarek Moselhy, Matthew Parno, and Alessio Spantini. Sampling via measure transport: An introduction. In *Handbook of Uncertainty Quantification*, pages 1–41. Springer, 2016.
- [24] N. Petra, J. Martin, G. Stadler, and O. Ghattas. A computational framework for infinite-dimensional Bayesian inverse problems, part ii: Stochastic Newton MCMC with application to ice sheet flow inverse problems. *SIAM Journal on Scientific Computing*, 36(4):A1525–A1555, 2014.
- [25] Aaditya Ramdas, Sashank Jakkam Reddi, Barnabás Póczos, Aarti Singh, and Larry Wasserman. On the decreasing power of kernel and distance based nonparametric hypothesis tests in high dimensions. In *Twenty-Ninth AAAI Conference on Artificial Intelligence*, 2015.
- [26] A.K. Saibaba, J. Lee, and P.K. Kitanidis. Randomized algorithms for generalized Hermitian eigenvalue problems with application to computing Karhunen–Loève expansion. *Numerical Linear Algebra with Applications*, 23(2):314–339, 2016.
- [27] Claudia Schillings and Christoph Schwab. Sparse, adaptive Smolyak quadratures for Bayesian inverse problems. *Inverse Problems*, 29(6):065011, 2013.
- [28] Claudia Schillings and Christoph Schwab. Scaling limits in computational Bayesian inversion. *ESAIM: Mathematical Modelling and Numerical Analysis*, 50(6):1825–1856, 2016.
- [29] Ch. Schwab and A.M. Stuart. Sparse deterministic approximation of Bayesian inverse problems. *Inverse Problems*, 28(4):045003, 2012.
- [30] A. Spantini, A. Solonen, T. Cui, J. Martin, L. Tenorio, and Y. Marzouk. Optimal low-rank approximations of Bayesian linear inverse problems. *SIAM Journal on Scientific Computing*, 37(6):A2451–A2487, 2015.
- [31] Dilin Wang, Zhe Zeng, and Qiang Liu. Stein variational message passing for continuous graphical models. In *International Conference on Machine Learning*, pages 5206–5214, 2018.
- [32] Yifei Wang and Wuchen Li. Information Newton’s flow: second-order optimization method in probability space. *arXiv preprint arXiv:2001.04341*, 2020.
- [33] Olivier Zahm, Tiangang Cui, Kody Law, Alessio Spantini, and Youssef Marzouk. Certified dimension reduction in nonlinear Bayesian inverse problems. *arXiv preprint arXiv:1807.03712*, 2018.
- [34] Jingwei Zhuo, Chang Liu, Jiaxin Shi, Jun Zhu, Ning Chen, and Bo Zhang. Message passing Stein variational gradient descent. In *International Conference on Machine Learning*, pages 6018–6027, 2018.

A Proof of Theorem 1

Proof. We first show (28). By definition of $\pi(w)$ in (20), we have

$$\nabla_w \log \pi(w) = \nabla_w \log(g(\Psi_r w)) + \nabla_w \log(\pi_0(w)). \quad (35)$$

For the second term, by definition of π_0 in (19), we have

$$\nabla_w \log(\pi_0(w)) = \nabla_w \log p_0^r(\Psi_r w) = \frac{\nabla_w p_0^r(\Psi_r w)}{p_0^r(\Psi_r w)}, \quad (36)$$

where by definition of $p_0^r(\Psi_r w)$ in (17) we have

$$\nabla_w p_0^r(\Psi_r w) = \int_{X_\perp} \nabla_w p_0(\Psi_r w + \xi) d\xi = \int_{X_\perp} \Psi_r^T \nabla_x p_0(\Psi_r w + \xi) d\xi = \Psi_r^T \nabla_x p_0^r(\Psi_r w). \quad (37)$$

The first term $\nabla_w \log(g(\Psi_r w))$ in (35) can be derived similarly by the definition of g in (16) and (17).

Next, we proceed to prove the equivalence (29) and (30) at the first step $\ell = 0$. Then the equivalence for steps $\ell > 0$ follows by induction. By the parameter decomposition $x = x^r + x^\perp$ with $x^r = P_r x$, we denote η_0 and η as the prior and posterior for the projected parameter x^r , given by

$$\eta_0(x^r) = p_0(P_r x) \text{ and } \eta(x^r) = p_r(P_r x), \quad (38)$$

where p_r is the projected density defined in (13) with optimal profile function $g = g$ given in (16). Equivalently, by the property of the projection $P_r P_r x = P_r x$, we have

$$\eta(x^r) = \frac{1}{Z_r} g(x^r) \eta_0(x^r). \quad (39)$$

We can write the transport map (4) for the projected parameter x^r in the steepest direction φ_0 as

$$T(x^r) = x^r + \epsilon \varphi_0(x^r), \quad (40)$$

where φ_0 is given by

$$\varphi_0(\cdot) = \mathbb{E}_{x^r \sim \eta_0} [\mathcal{A}_\eta \kappa(x^r, \cdot)], \quad (41)$$

with the kernel $\kappa(x^r, \tilde{x}^r) = k(P_r x, P_r \tilde{x})$ for any $x, \tilde{x} \in \mathbb{R}^d$ and the Stein operator

$$\mathcal{A}_\eta \kappa(x^r, \cdot) = \nabla_{x^r} \log \eta(x^r) \kappa(x^r, \cdot) + \nabla_{x^r} \kappa(x^r, \cdot). \quad (42)$$

By definition of the kernel in (9), we have

$$\begin{aligned} & k(P_r x, P_r \tilde{x}) \\ &= \exp \left(-\frac{1}{h} (P_r x - P_r \tilde{x})^T (P_r x - P_r \tilde{x}) \right) \\ &= \exp \left(-\frac{1}{h} (w - \tilde{w})^T \Psi_r^T \Psi_r (w - \tilde{w}) \right) \\ &= \exp \left(-\frac{1}{h} \|w - \tilde{w}\|_2^2 \right) \end{aligned} \quad (43)$$

where we used the relation $P_r x = \Psi_r w$ and $P_r \tilde{x} = \Psi_r \tilde{w}$ in the second equality and the orthonormality $\Psi_r^T \Psi_r = I$ in the generalized eigenvalue problem (11) in the third. Therefore, by definition (27), we have

$$k^r(w, \tilde{w}) = \kappa(x^r, \tilde{x}^r). \quad (44)$$

Moreover, for the gradient of the kernel we have

$$\begin{aligned} \nabla_{x^r} \kappa(x^r, \tilde{x}^r) &= -\frac{2}{h} \kappa(x^r, \tilde{x}^r) (x^r - \tilde{x}^r) \\ &= -\frac{2}{h} \kappa(x^r, \tilde{x}^r) \Psi_r (w - \tilde{w}). \end{aligned} \quad (45)$$

On the other hand, we have

$$\nabla_w k^r(w, \tilde{w}) = -\frac{2}{h} k^r(w, \tilde{w}) (w - \tilde{w}), \quad (46)$$

which yields

$$\nabla_w k^r(w, \tilde{w}) = \Psi_r^T \nabla_{x^r} \kappa(x^r, \tilde{x}^r). \quad (47)$$

For the posterior η defined in (38), we have

$$\nabla_{x^r} \log \eta(x^r) = \frac{\nabla_{x^r} (g(x^r) \eta_0(x^r))}{g(x^r) \eta_0(x^r)}, \quad (48)$$

while for the posterior π defined in (20), we have

$$\nabla_w \log \pi(w) = \frac{\nabla_w (g(\Psi_r w) \pi_0(w))}{g(\Psi_r w) \pi_0(w)}. \quad (49)$$

By chain rule, it is straightforward to see that

$$\nabla_w g(\Psi_r w) = \Psi_r^T \nabla_{x^r} g(x^r). \quad (50)$$

Under assumption $\pi_0(w) = p_0(P_r x)$ in Theorem 1, and $p_0(P_r x) = \eta_0(x^r)$ by definition (38), we have

$$\nabla_w \pi_0(w) = \Psi_r^T \nabla_{x^r} \eta_0(x^r). \quad (51)$$

Therefore, combining (50) and (51), we have

$$\nabla_w \log \pi(w) = \Psi_r^T \nabla_{x^r} \log \eta(x^r). \quad (52)$$

To this end, we obtain the equivalence of the Stein operators

$$\mathcal{A}_\pi k^r(w, \tilde{w}) = \Psi_r^T \mathcal{A}_\eta \kappa(x^r, \tilde{x}^r) \quad (53)$$

for $x^r = \Psi_r w$ and $\tilde{x}^r = \Psi_r \tilde{w}$. Since the prior densities $\eta_0(x^r) = \pi_0(w)$, we have the equivalence

$$\mathbb{E}_{w \sim \pi_0} [\mathcal{A}_\pi k^r(w, \tilde{w})] = \Psi_r^T \mathbb{E}_{x^r \sim \eta_0} [\mathcal{A}_\eta \kappa(x^r, \tilde{x}^r)], \quad (54)$$

which concludes the equivalence of the transport map (29) by $w = \Psi_r^T x^r$ with the same ϵ at $\ell = 0$. Moreover, by induction we have

$$T_\ell^r(w^\ell) = \Psi_r^T T_\ell(P_r x^\ell), \quad (55)$$

which concludes. □

B A linear inference problem

This example is presented to test the accuracy of the proposed algorithm with analytically given posterior distribution for a linear inference problem. We consider a linear parameter-to-observable map $A : \mathbb{R}^d \rightarrow \mathbb{R}^s$, which is given by

$$Ax = O \circ Bx, \quad (56)$$

where $B : x \rightarrow u$ is a linear discrete solution map of the diffusion reaction equation (Δ is the Laplace operator)

$$-\Delta u + u = x, \quad \text{in } (0, 1), \quad (57)$$

with boundary condition $u(0) = 0$ and $u(1) = 1$, which is solved by a finite element method. The continuous parameter x and solution u are discretized by finite elements with piecewise linear elements in a uniform mesh of size d . $x \in \mathbb{R}^d$ and $u \in \mathbb{R}^d$ are the nodal values of x and u . The parameter x is assumed to follow a Gaussian distribution $\mathcal{N}(0, \mathcal{C})$ with covariance $\mathcal{C} = (-0.1\Delta + I)^{-1}$, which leads to a Gaussian parameter $x \sim \mathcal{N}(0, \Sigma_x)$, with covariance $\Sigma_x \in \mathbb{R}^{d \times d}$ as a discretization of \mathcal{C} .

$O : \mathbb{R}^d \rightarrow \mathbb{R}^s$ in (56) is an observation map that take s components of u that are equally distributed in $(0, 1)$. For $s = 15$, we have $Ou = (u(1/16), \dots, u(15/16))^T$. We assume an additive 1% Gaussian noise $\xi \sim \mathcal{N}(0, \Sigma_\xi)$ with $\Sigma_\xi = \sigma^2 I$ and $\sigma = \max(|Ou|)/100$ for data

$$y = Ax + \xi, \quad (58)$$

then the likelihood function is given by

$$f(x) = \exp\left(-\frac{1}{2}\|y - Ax\|_{\Sigma_\xi}^2\right). \quad (59)$$

Because of the linearity of the inference problem, the posterior of x is also Gaussian $\mathcal{N}(x_{\text{MAP}}, \Sigma_y)$ with the MAP point $x_{\text{MAP}} = \Sigma_y A^T \Sigma_\xi^{-1} y$ and covariance

$$\Sigma_y = (A^T \Sigma_\xi^{-1} A + \Sigma_x^{-1})^{-1}. \quad (60)$$

We run SVGD and pSVGd (projection with $r = 8$ basis functions and $\lambda_9 < 10^{-4}$) with 256 samples and 200 iterations for different dimensions, both using line search to seek the step size ϵ_ℓ . The RMSE (of 10 trials and their average) of the samples variances compared to the ground truth (60) are shown in Figure 5, which indicates that SVGD deteriorates with increasing dimension while pSVGd performs well for all dimensions.

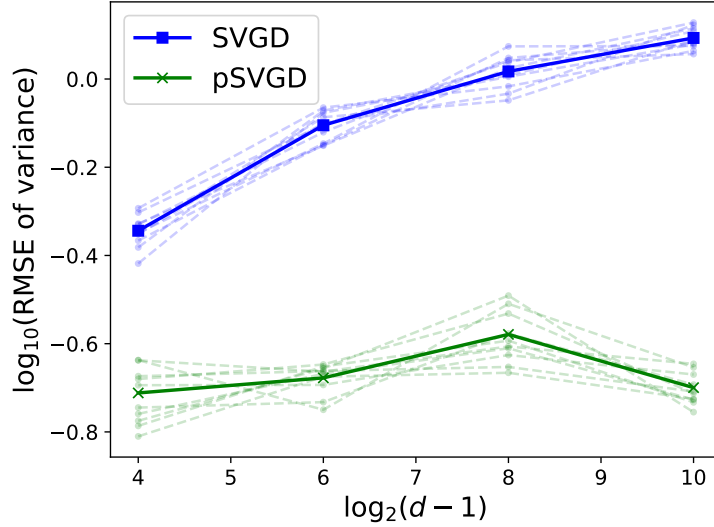


Figure 5: RMSE of pointwise sample variance in L_2 -norm, with 256 samples, SVGD and pSVGd both terminated at $\ell = 200$ iterations, parameter dimension $d = 2^n + 1$, with $n = 4, 6, 8, 10$.

C Application in COVID-19

Social distancing has played a key role in flattening the curve of the spread of COVID-19. In this example, we apply pSVGd to infer a time-dependent parameter that describes the contact reduction effect of social distancing given observation data. We consider a compartmental model with 8 compartments for the modeling of the transmission and outcome of COVID-19, as illustrated by the diagram in Figure 6, which is given by the system of ordinary differential equations

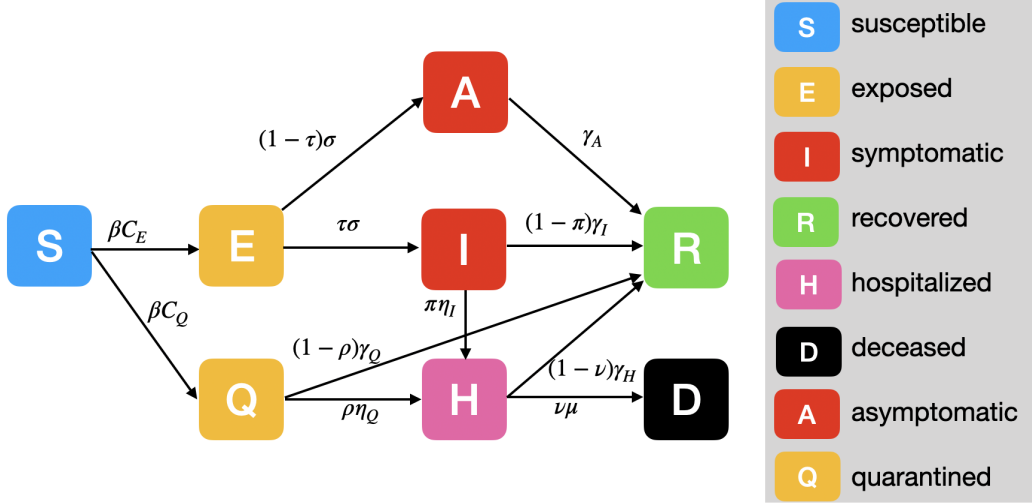


Figure 6: Sketch of a compartmental epidemic model with 8 compartments for modeling of transmission and outcome of infectious diseases such as COVID-19.

$$\begin{aligned}
C_E(t) &= (1 - \alpha(t))(1 - q) \frac{I(t)}{N} + (1 - \alpha(t)) \frac{A(t)}{N}, \\
C_Q(t) &= (1 - \alpha(t))q \frac{I(t)}{N}, \\
\frac{dS(t)}{dt} &= -\beta C_E(t)S(t) - \beta C_Q(t)S(t), \\
\frac{dE(t)}{dt} &= \beta C_E(t)S(t) - \tau\sigma E(t) - (1 - \tau)\sigma E(t), \\
\frac{dQ(t)}{dt} &= \beta C_Q(t)S(t) - \rho\eta_Q Q(t) - (1 - \rho)\gamma_Q Q(t), \\
\frac{dA(t)}{dt} &= (1 - \tau)\sigma E(t) - \gamma_A A(t), \\
\frac{dI(t)}{dt} &= \tau\sigma E(t) - \pi\eta_I I(t) - (1 - \pi)\gamma_I I(t), \\
\frac{dH(t)}{dt} &= \pi\eta_I I(t) + \rho\eta_Q Q(t) - \nu\mu H(t) - (1 - \nu)\gamma_H H(t), \\
\frac{dR(t)}{dt} &= \gamma_A A(t) + (1 - \pi)\gamma_I I(t) + (1 - \nu)\gamma_H H(t) + (1 - \rho)\gamma_Q Q(t), \\
\frac{dD(t)}{dt} &= \nu\mu H(t).
\end{aligned} \tag{61}$$

In this model, $\alpha(t) \in [0, 1]$ represents the effective contact reduction of social distancing at time t , i.e., the percentage of reduced contact compared to the status without social distancing, which is the time-dependent parameter we infer. Briefly on the other parameters, N is the total population for a given region, β is a transmission rate, q is quarantined rate, σ is latency rate, η_I, η_Q are hospitalized rates, $\gamma_A, \gamma_I, \gamma_Q, \gamma_H$ are recovery rates, μ is deceased rate, τ, ρ, π, ν are the proportions of cases going from E to I , Q to H , I to H , and H to D . We assume these parameters are scalar and do not change over time. We use the number of hospitalized cases H (7 days' moving average) in New York available in <https://github.com/COVID19Tracking> as the observation data and assume that the observation noise is i.i.d. $N(0, 1)$ for the logarithm of the data to create the likelihood function.

First, we deterministically infer all these parameters by solving an optimization problem to minimize the misfit between the logarithm of the predicted number of hospitalized cases and that of the observed

number. Then we freeze all the parameters at their optimal values except for $\alpha(t)$. We assume that

$$\alpha(t) = \frac{1}{2}(\tanh(x(t)) + 1)$$

is a stochastic process with Gaussian process $x(t) \sim \mathcal{N}(\hat{x}(t), \mathcal{C})$, where $\hat{x}(t) = \operatorname{arctanh}(2\hat{\alpha}(t) - 1)$ at the deterministic optimal values of the social distancing $\hat{\alpha}(t)$ obtained from the deterministic optimization problem, $\mathcal{C} = -(\delta\Delta_t)^{-1}$ with Laplacian operator Δ_t and a scaling parameter $\delta = 10$. After discretization in time with step of one day over 96 days, we obtain a discrete parameter $x = (x_1, \dots, x_d)$ of dimension $d = 96$. We run pSVGD and SVGD with line search, 128 samples with 8 samples in each of 16 processor cores, update the bases for pSVGD every 10 iterations for a total of 200 iterations. The results are shown in Figure 7. We can observe a fast decay of eigenvalues and a small number of intrinsic dimension. The bottom two figures display the samples, their mean, and 90% confidence interval of the reduction factor α for social distancing and the number of hospitalized cases by SVGD (top) and pSVGD (bottom). We can observe that pSVGD provides much more accurate prediction of the data (the number of hospitalized cases) with tighter confidence interval than SVGD from the right of Figure 7. Meanwhile, the mean of the pSVGD samples of the reduction factor α of social distancing is much closer to the deterministic optimal value than that of SVGD, with 90% confidence interval of pSVGD covering the deterministic optimal value, while that of SVGD not. The mean of the reduction factor α for SVGD is nearly 1 for a period of time, which corresponds to complete shutdown without any transmission, which is not realistic.

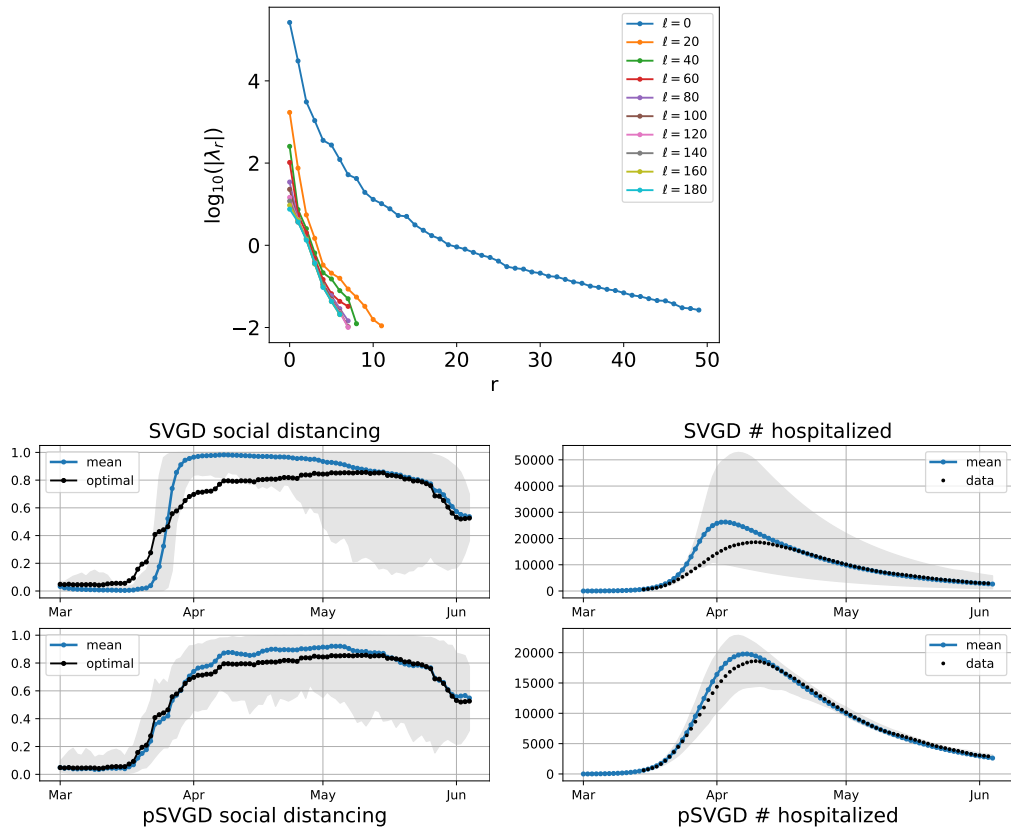


Figure 7: Top: Decay of the eigenvalues of (11) at different iteration numbers ℓ . Bottom-left: samples of the reduction factor α of social distancing, posterior mean, 90% confidence interval in shadow, deterministic optimal $\hat{\alpha}$. Bottom-right: the number of hospitalized cases, posterior mean, 90% confidence interval in shadow, and reported data for New York. The results are at iteration $\ell = 200$.